Low Temperature Physics/Fizika Nizkikh Temperatur, 2012, v. 38, No. 1, pp. 28–38

Excess conductivity of $Cu_{0.5}Tl_{0.5}Ba_2Ca_3Cu_{4-y}Zn_yO_{12-\delta}$ superconductors

Nawazish A. Khan and S.M. Hasnain

Materials Science Laboratory, Department of Physics, Quaid-i-Azam University, Islamabad 45320, Pakistan
E-mail: nawazishalik2@yahoo.com

Received June 20, 2011, revised July 19, 2011

Oxide high-T_c superconductors (HTSC) are anisotropic in character since the charge carriers have free moment in the conducting CuO_2 planes [1] whereas their motion is impeded by insulating/partially insulating $MBa_2O_{4-\delta}$ (M = Y, Bi, Hg, Tl, CuTl, etc.) charge reservoir layers. In the transport process the charge carriers have to tunnel across insulating/partially insulating barriers along the *c*-axis and across the grain boundaries, which promote a fluctuation in the order parameter and in turn to the conductivity of the carriers. The studies of such fluctuation conductivity (FIC) may help in understanding the intrinsic mechanism of superconductivity. Here the electrical resistivity $\rho(T)$ versus temperature data of as-prepared and oxygen post-annealed $Cu_{0.5}Tl_{0.5}Ba_2Ca_3Cu_{4-y}Zn_yO_{12-\delta}$ (y = 0, 0.5, 1.5, 2.5) samples is studied for FIC analyses in the temperature regime well above the critical temperature; such analyses have been carried out by employing Lawrence and Doniach (LD) and Maki–Thompson (MT) models. The coherence length, inter-plane coupling, exponent, dimensionality of fluctuations and the phase relaxation time of the carriers are determined from such analyses. It is observed that the crossover temperature associated with two distinct exponents fits very well with the two-dimensional (2D) and three-dimensional (3D) LD equations. The crossover temperature T_0 is shifted to higher temperatures with enhanced Zn doping. The 3D LD region is shifted to higher temperature with the increased Zn doping. We have elucidated from these analyses that lower Tl content in the final compound may increase the charge carrier's doping efficiency of $MBa_2O_{4-\delta}$ charge reservoir layer, resulting into an increase in the coherence length along the *c*-axis and superconductivity parameters. A small decrease in the coherence length along the *c*-axis $\xi_c(0)$ is observed in the samples with Zn doping of y = 1.5 whereas $\xi_c(0)$ increases in the samples y = 0.5, 2.5. In comparison with as-prepared samples, the $\xi_c(0)$ decreases after post-annealing in oxygen atmosphere. It is most likely that a decrease in the density of charge carrier's is promoted by oxygen diffusion in the unit cell may suppress the $\xi_c(0)$. The increase oxygen diffusion is evidenced from the softening of phonon modes after post-annealing in oxygen atmosphere. The decreased population of small spins of Cu atoms induced by doping of Zn is viewed in the terms of suppression of spin gap and hence the pseudo-gap in $Cu_{0.5}Tl_{0.5}Ba_2Ca_3Cu_{4-y}Zn_yO_{12-\delta}$ (y = 0, 0.5, 1.5, 2.5) samples.

PACS: **74.70.–b** Superconducting materials other than cuprates;
74.72.Jt Other cuprates, including Tl and Hg-based cuprates;
74.62.Bf Effects of material synthesis, crystal structure, and chemical composition.

Keywords: excess conductivity analyses, increase in coherence length with Zn-doping, phonon modes softening with Zn-doping, suppression of pseudo-gap.

1. Introduction

The fluctuation induces conductivity in oxide HTSC plays a very vital role in the understanding of intrinsic properties of a material. These fluctuations in the order parameter set in at the temperatures well above the critical temperature T_c, which in turn gives rise to excess conductivity. One of the reasons for the higher T_c in oxide HTSC's is their excess conductivity resulting out of formation of the Cooper pairs well above the critical temperature. The formation of these Cooper pairs is local [1,2] and at the critical temperature of a compound a steady state generation rate of cooper pair formation dominates the rate at which these Cooper pairs are broken down. The formation of Cooper pairs well above the critical temperature imparts additional conductivity in the resistivity versus temperature measurements. The two main route causes of excess conductivity are the Cooper pair formation well

above the critical temperature and the additional conductivity due to these pairs is explained by Aslamazov–Larkin (AL) equations [3] in thin films samples and by Lawrence–Doniach (LD) model in polycrystalline samples [4]. Through the analysis of resistivity versus temperature data, a crossover temperature T_0 may be predicted. At this temperature the 2D and 3D competing conductivity processes Cooper pair meet. The system transforms from more isotropic three dimensional (3D) electronic state to a two dimensional (2D) an-isotropic state with increase of temperature. In oxide superconductors with conducting CuO_2, the AL term dominates close to T_c. Since the formation of Cooper pair takes place in the background of normal electrons, the effect of superconducting fluctuations on the conductivity of normal electrons explained by Maki–Thompson (MT) term [5]. The MT part depends on the phase-relaxation time t_φ and becomes significant in 2D fluctuations regime accompanied by moderate pair-breaking [6]. The excess conductivity is, given by:

$$\sigma'(T) = \left[\frac{\rho_N(T) - \rho(T)}{\rho_N(T)\rho(T)}\right]. \qquad (1)$$

In this equation the $\rho(T)$ is the actually measured resistivity and $\rho_N(T) = \alpha + \beta T$ $[\rho_N(T) = 1/\sigma_N(T)]$ is the extrapolated normal state resistivity to zero Kelvin; the α is a intercept and β is a slope of straight line. The analysis of experimentally observed data for FIC helps in understanding the intrinsic microscopic properties responsible for mechanism of high temperature superconductivity. Through the analysis of resistivity versus temperature data for FIC one can determine the reliable values of $\xi_c(T)$, t_φ, and dimensionality of conductivity. Since the carriers in oxide HTSC's have very short Ginzburg–Landau coherence length $\xi_{GL}(0)$, it is advisable to carry out FIC analysis of temperature dependent conductivity $\Delta\sigma(T) = \Delta\sigma_{RT}\varepsilon^{-\lambda}$ analysis of data well above the T_c. The analysis is done via:

$$\ln \sigma'(T) = \ln \Delta\sigma_{RT} - \lambda_D \ln(\varepsilon), \qquad (2)$$

where $\varepsilon = (T - T_c^{mf})/T_c^{mf}$ with T_c^{mf} determined from the peak value of derivative of resistivity in the transition region and λ_D is dimensional exponent equal to −0.5 for 3D behavior, −1.0 for 2D, and −2.0 for zero dimension (0D) corresponding to the formation and breaking down of the Cooper pairs instantly with no sense in any direction. The dimensionality and exponent of it follow the relationship: Dimensionality = $2(2+\lambda_D)$ [7].

The excess conductivities analysis for $YBa_2Cu_3O_{7-\delta}$ superconductors have been carried out both on bulk and thin films samples. In the fitting schemes mentioned in these articles the polycrystalline bulk samples have shown 3D fluctuations in the neighborhood of transition region associated with a cross to 2D-dimensional thermal fluctuations [8–11]. The thin films YBaCO samples have shown a mix of 2D to 3D regimes associated with a crossover at a particular temperature T_0 [11]. The excess conductivity analyses of $Bi_2Sr_2Ca_{n-1}Cu_nO_x$ (n = 2, 3) superconductors have shown 3D excess conductivity closer to the transition temperature whereas 2D conductivity regimes extended to over much higher temperatures above T_c [12–15].

The doping of impurity atoms at the Cu-sites in the CuO_2 planar sites is very efficient tool for the understanding of intrinsic mechanism of superconductivity in oxide HTSC. In the previous studies on copper oxide based high temperature superconductors, the critical temperature is found to be significantly decreasing with the doping of Zn [16–24]. The suppression of T_c with Zn^{+2} doping at CuO_2 planar sites in *d*-wave HTSC's atoms is unique and is proposed in the previous studies to be arising from the pair breaking mechanism or electronic localization induced by doped atoms [19–24]. We have also carried out doping of Zn at CuO_2 planar sites in $Cu_{0.5}Tl_{0.5}Ba_2Ca_3Cu_4O_{12-\delta}$ superconductors. Contrary to all the previous studies we have observed enhanced superconductivity in Zn-doped $Cu_{0.5}Tl_{0.5}Ba_2Ca_3Cu_{4-y}Zn_yO_{12-\delta}$ (y = 0, 0.5, 1.5, 2.5) [CuTlZn-1234] superconductors [26]. In this paper we continue the study of CuTlZn-1234 superconductors via FIC analyses to find out route causes of this unusual behavior and to shed light on the underlying mechanism of superconductivity in this compound.

2. Experimental

The $Cu_{0.5}Tl_{0.5}Ba_2Ca_3Cu_{4-y}Zn_yO_{12-\delta}$ (y = 0, 0.5, 1.5, 2.5) samples were prepared by the solid state reaction method accomplished in two stages. At the first stage $Cu_{0.5}Ba_2Ca_3Cu_{4-y}Zn_yO_{12-\delta}$ precursor material was prepared, by thoroughly mixing ZnO, $Ba(NO_3)_2$, $Ca(NO_3)_2$ and Cu(CN) in a quartz mortar and pestle in appropriate ratios. The mixed material was fired twice at 900 °C in a quartz boat for 24 h and furnace cooled to room temperature. At the second stage, the precursor material was ground for about an hour and mixed with Tl_2O_3 to give $Cu_{0.5}Tl_{0.5}Ba_2Ca_3Cu_{4-y}Zn_yO_{12-\delta}$ (y = 0, 0.5, 1.5, 2.5) as final reactants composition. Thallium mixed material was palletized under 3.8 tons/cm^2 and the pellets were enclosed in a gold capsule. Gold capsule containing pellets were annealed for about 10 min at 900 °C followed by quenching to room temperature. The samples were characterized by resistivity, ac-susceptibility and critical current density measurements. The structure of the material was determined by x-ray diffraction scan from Rigaku D/Max IIIC, using a CuKα source of wavelength 1.54056 Å and the cell parameters were determined by a cell refinement computer program. The phonon modes related to the vibrations of various oxygen atoms in $Cu_{0.5}Tl_{0.5}Ba_2Ca_3Cu_{4-y}Zn_yO_{12-\delta}$ unit cell were observed by Nicolet 5700 Fourier Transform Infrared Spectrometer (FTIR) in 400–700 cm^{-1} wave number range. The post-annealing of the samples in flowing

oxygen atmosphere was carried out in a tubular furnace at 500°C for six hours.

3. Results and discussion

3.1. Resistivity and susceptibility measurements

The x-ray diffraction scans of superconductor samples $Cu_{0.5}Tl_{0.5}Ba_2Ca_3Cu_{4-y}Zn_yO_{12-\delta}$ (y = 0.5, 1.5, 2.5) are shown in Fig. 1. These samples have shown tetragonal structure following *P*4/*mmm* space group; length of *a*-axis increases whereas *c*-axis decreases with increased Zn-doping. The resistivity measurements of as-prepared $Cu_{0.5}Tl_{0.5}Ba_2Ca_3Cu_{4-y}Zn_yO_{12-\delta}$ (y = 0, 0.5, 1.5, 2.5) samples are shown in Fig. 2,*a*. A metallic variation of resistivity from room temperature down to onset of superconductivity is witnessed in all these samples. These samples have shown onset of the superconductivity around 113.2, 117.4, 125.2 and 123.4 K and the $T_c(R = 0)$ around 99.3, 103.4,

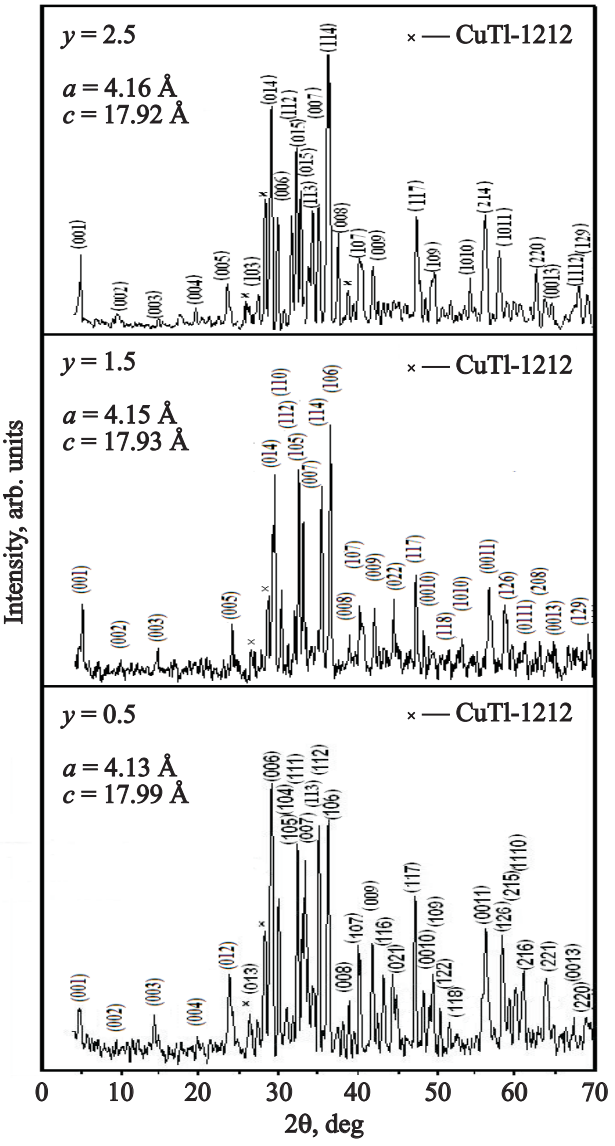

Fig. 1. X-ray diffraction pattern of $Cu_{0.5}Tl_{0.5}Ba_2Ca_3Cu_{4-y}Zn_yO_{12-\delta}$ (y = 0.5, 1.5, 2.5) superconductor samples.

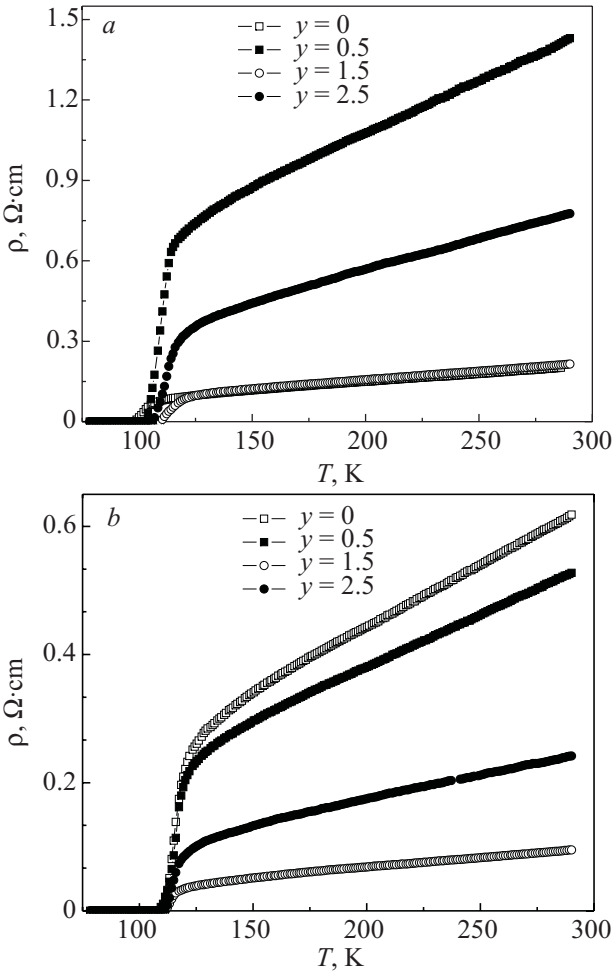

Fig. 2. Resistivity vs temperature plot of as prepared $Cu_{0.5}Tl_{0.5}Ba_2Ca_3Cu_{4-y}Zn_yO_{12-\delta}$ (y = 0, 0.5, 1.5, 2.5) samples (*a*). Resistivity vs temperature plot of as oxygen annealed $Cu_{0.5}Tl_{0.5}Ba_2Ca_3Cu_{4-y}Zn_yO_{12-\delta}$ (y = 0, 0.5, 1.5, 2.5) samples (*b*).

110.4 and 106.6 K for Zn-doping y = 0, 0.5, 1.5, 2.5 in $Cu_{0.5}Tl_{0.5}BaCa_3Cu_{4-y}Zn_yO_{12-\delta}$, respectively. These measurements for the oxygen post-annealed samples are shown in Fig. 2,*b*. Oxygen post-annealed samples have also shown metallic variation of resistivity down to onset of superconductivity. The onset of superconductivity in these samples is observed around 128.3, 126.1, 125.1 and 127.4 K and the $T_c(R = 0)$ around 111.4, 109.4, 112.3 and 112.3 K, respectively.

Ac-susceptibility measurements of these samples are shown in the inset of Fig. 3,*a* and Fig. 3,*b*. In as-prepared samples the onset of diamagnetism is observed around 126.1, 124.3, 124.8 and 125.3 K, respectively, Fig. 3,*a*. The magnitude of diamagnetism decreases for the samples with Zn doping of y = 0.5, 1.5 whereas it is recovered to the value observed in un-doped samples with Zn doping of y = 2.5. These samples have shown peak temperature in the out-of-phase component of magnetic susceptibility around 111.7, 113.9, 119.5 and 115.3 K. Oxygen post-annealed samples have shown onset of diamagnetic transition

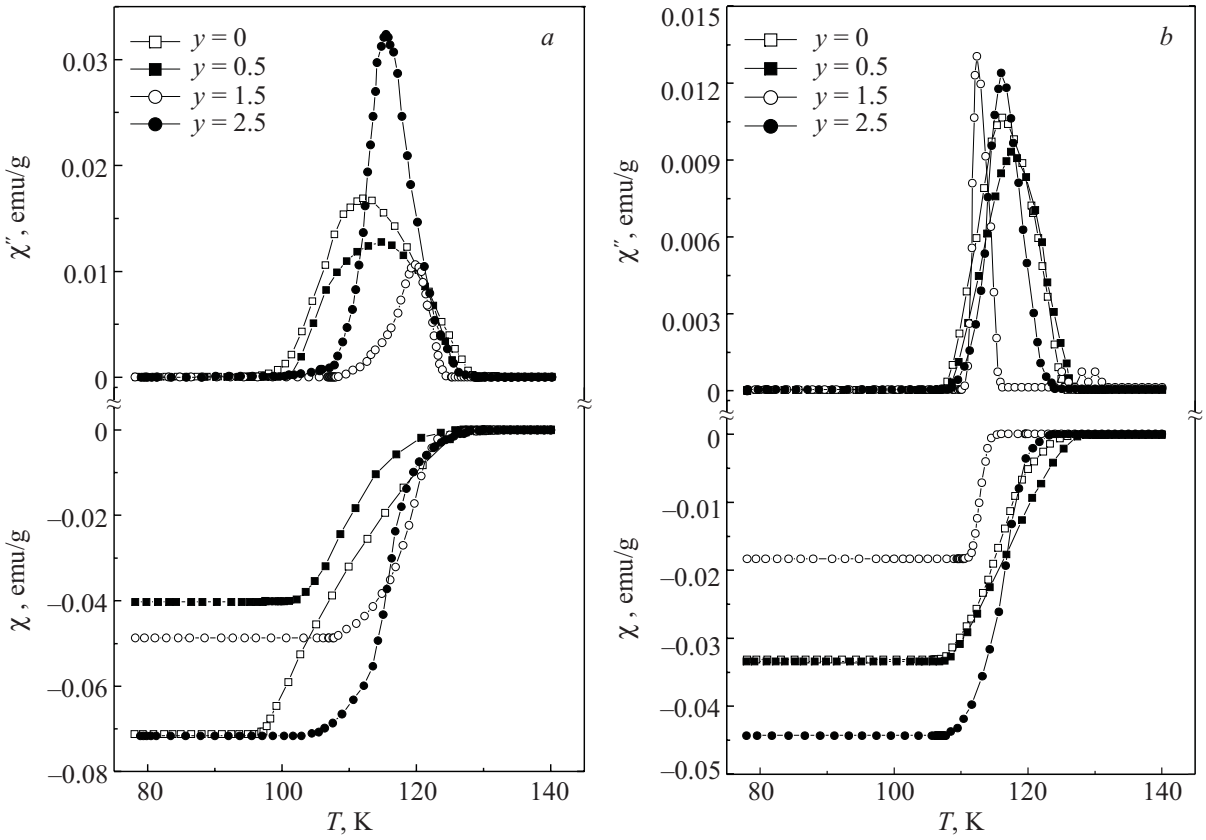

Fig. 3. AC-susceptibility ($B = 0$) of as-prepared $Cu_{0.5}Tl_{0.5}Ba_2Ca_3Cu_{4-y}Zn_yO_{12-\delta}$ ($y = 0$, 0.5, 1.5, 2.5) samples, showing onset diamagnetic temperatures (*a*). AC-susceptibility ($B = 0$) of oxygen annealed $Cu_{0.5}Tl_{0.5}Ba_2Ca_3Cu_{4-y}Zn_yO_{12-\delta}$ ($y = 0$, 0.5, 1.5, 2.5) samples, showing onset diamagnetic temperatures (*b*).

around 125.1, 127.1, 114.7, 122.6 K and a peak temperature in the out-of-phase component magnetic susceptibility around 116.2, 117.3, 112.2 and 116 K, respectively, Fig. 3,*b*. Compare with as-prepared samples the magnitude of diamagnetism is decreased in all samples after post-annealing in oxygen.

3.2. FTIR absorption measurements

Oxygen related phonon modes in high temperature superconductors $Cu_{0.5}Tl_{0.5}Ba_2Ca_{n-1}Cu_{n-y}Zn_yO_{2n+4-\delta}$ ($n = 3$, 4) are observed in the wavenumber range 400 to 700 cm^{-1}. The phonon modes related to the vibrations of apical oxygen of type Tl-O_A-M(2) and Cu(1)-O_A-Cu(2) have been observed in the wave number range 400–480 cm^{-1} and 480–540 cm^{-1}, respectively. The CuO_2 planar oxygen mode has previously been observed in the wave number range 573–578 cm^{-1}. The position of center of these bands critically depends on the oxygen and thallium contents in the final compound. It is important to note that center of band of all the phonon modes in these 900 °C synthesized samples is at relatively higher wave numbers in comparison with the same composition of the samples synthesized at 880 °C [25,26]. The most likely reason for the softening of all phonon modes related to the vibrations of various oxygen atoms in the present studies is the lower thallium and oxygen contents in the $Cu_{0.5}Tl_{0.5}Ba_2O_{4-\delta}$ charge reservoir layer of these samples. Hardening of phonon modes YBaCuO samples with lower oxygen contents in the charge reservoir had also been witnessed in previous studies [27]. FTIR absorption spectra observed for $Cu_{0.5}Tl_{0.5}Ba_2Ca_3Cu_{4-y}Zn_yO_{12-\delta}$ ($y = 0$, 0.5, 1.5, 2.5) samples are shown in Fig. 4,*a*. In un-doped $Cu_{0.5}Tl_{0.5}Ba_2Ca_3Cu_4O_{12-\delta}$ samples, the apical oxygen mode of type Tl-O_A-Cu(2)/Zn is observed around 400–492 cm^{-1}. The position of this band with varying intensity remains the same in all Zn-doped $Cu_{0.5}Tl_{0.5}Ba_2Ca_3Cu_{4-y}Zn_yO_{12-\delta}$ ($y = 0.5$, 1.5, 2.5) samples. The Cu(1)-O_A-Cu(2)/Zn mode in Zn un-doped sample is peaked around 539 cm^{-1}. This mode is softened with increased Zn doping and is observed around 538, 536 and 535 cm^{-1} in Zn-doped $Cu_{0.5}Tl_{0.5}Ba_2Ca_3Cu_{4-y}Zn_yO_{12-\delta}$ ($y = 0.5$, 1.5, 2.5) samples. The CuO_2 planar mode in zinc un-doped sample is observed around 607 cm^{-1}. This CuO_2/ZnO_2 planar mode is also softened with the doping of Zn and is observed around 606, 605, 604 cm^{-1} in Zn-doped $Cu_{0.5}Tl_{0.5}Ba_2Ca_3Cu_{4-y}Zn_yO_{12-\delta}$ ($y = 0$, 0.5, 1.5, 2.5) samples. The O_δ mode of oxygen atoms in the charge reservoir layer is observed around 689–692 cm^{-1}.

The FTIR absorption measurements of oxygen post-annealed $Cu_{0.5}Tl_{0.5}Ba_2Ca_3Cu_{4-y}Zn_yO_{12-\delta}$ ($y = 0$, 0.5, 1.5, 2.5) samples can be seen in Fig. 4,*b*. The peak position of all the modes, except O_δ mode of charge reservoir layer around ~692 cm^{-1}, is softened after post-annealing in oxy-

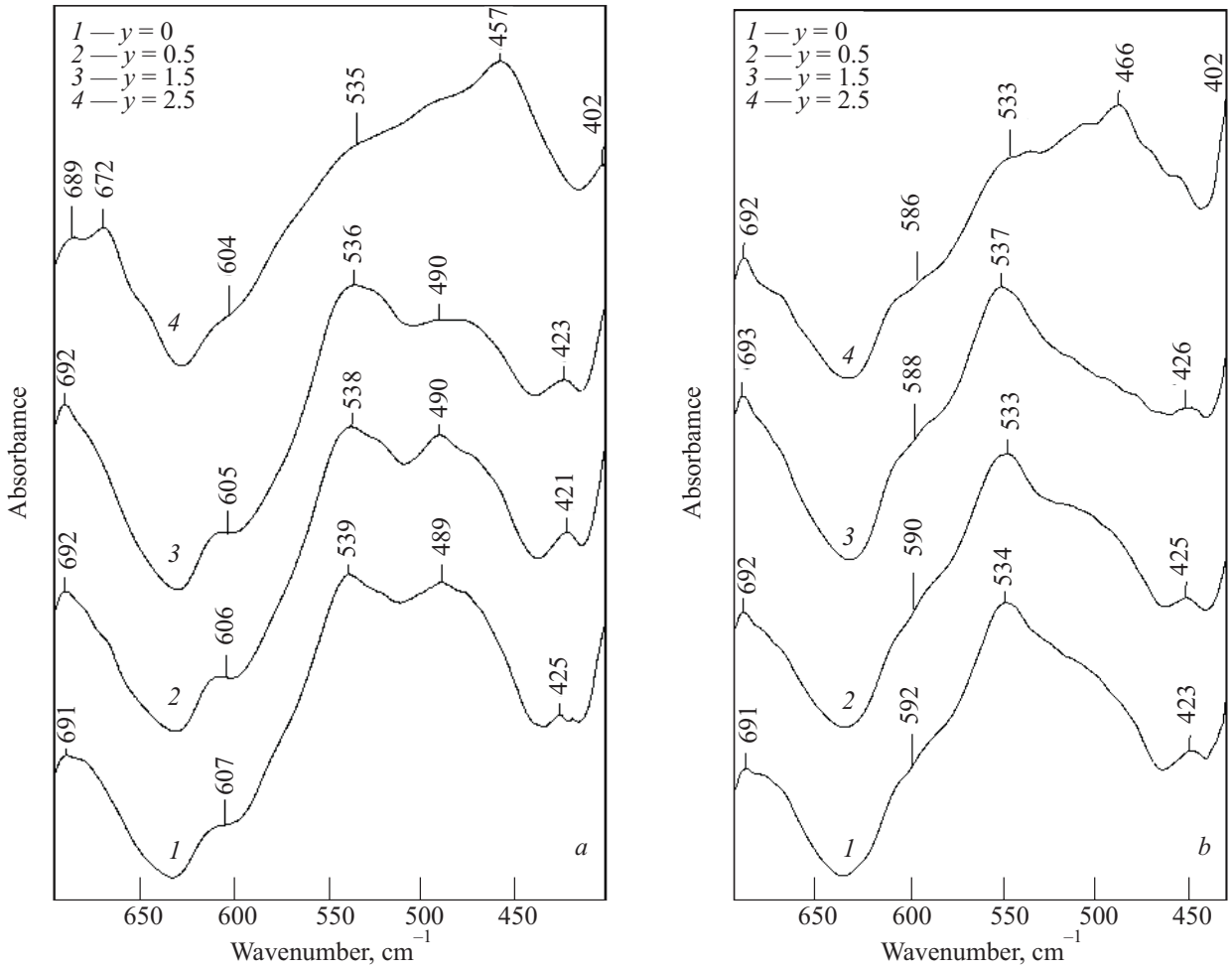

Fig. 4. FTIR of as prepared $Cu_{0.5}Tl_{0.5}Ba_2Ca_3Cu_{4-y}Zn_yO_{12-\delta}$ (y = 0, 0.5, 1.5, 2.5) samples (*a*). FTIR of oxygen annealed $Cu_{0.5}Tl_{0.5}Ba_2Ca_3Cu_{4-y}Zn_yO_{12-\delta}$ (y = 0, 0.5, 1.5, 2.5) samples (*b*).

gen. The apical oxygen mode of type Cu(1)-O_A-Cu(2)/Zn is observed around 534, 533, 537, 533 cm^{-1} in $Cu_{0.5}Tl_{0.5}Ba_2Ca_3Cu_{4-y}Zn_yO_{12-\delta}$ (y = 0, 0.5, 1.5, 2.5) samples. The CuO_2 planar mode in these samples is observed around 592, 590, 588, 586 cm^{-1}. However, O_δ mode of oxygen atoms of $Cu_{0.5}Tl_{0.5}Ba_2O_{4-\delta}$ charge reservoir layer is observed at its usual position around 691–693 cm^{-1}. It is most likely that the hardening of apical oxygen modes in 900 °C synthesized samples and their softening after post-annealing in oxygen is an evidence of lower oxygen and thallium contents in the final compound.

3.3. Excess conductivity analysis

The expression of Lawrence and Doniach model has been used for the analysis of our experimental results:

$$\sigma'(T)_{LD} = [e^2/(16\hbar d)](1+2\alpha)^{-1/2}\,\varepsilon^{-1}, \qquad (3)$$

where $\alpha = 2\xi_c^2(T)/d^2 = 2[\xi_c(0)/d]^2\varepsilon^{-1}$ is a coupling parameter [6]. Usually the LD model equation (1) gives the smooth curve (not the straight line) which can be approximated by straight lines with $\lambda = -0.5$ and $\lambda = -1$ only at the low temperature end and at the high temperature end of the range, respectively. After the FIC prediction by Aslamazov and Larkin [3] a huge amount of papers was published in which the 2D AL term given by

$$\sigma'_{AL} = \{e^2/[16\hbar d]\}\varepsilon^{-1}. \qquad (4)$$

But it has to be emphasized that all these publications were carried out using thin films prepared from conventional superconductors (CSC). In the case of such films $W \gg \xi(T)^3 d_0$, where W is the film width, d_0 is its thickness and $\xi(T)$ is a coherence length which is isotropic in CSC. In high-T_c superconductors (HTS's) $\xi(T)$ is the least and it is always $W > d_0 \gg \xi_{ab}(T) > \xi_c(T)$; for optimally doped YBCO samples $\xi_{ab}(0) \approx 13$ Å is the coherence length in the *ab* plane which is about ten times $\xi_c(0)$. Therefore, only very close to T_c, where $\xi(T)$ is getting extremely large {as $\xi(T) = \xi(0)(T/T_c - 1)^{-1/2}$}, the 3D AL superconductivity described by

$$\sigma'_{AL} = \{e^2/[32\hbar\xi_c(0)]\}\varepsilon^{-1/2} \qquad (5)$$

is realized and here $W > \xi_c(T) \gg d$; the d is the separation between conducting layers in HTS's [6]. With $T_0 = T_c\left[1+(2\xi_c(0)/d)^2\right]$ is 3D to 2D cross-over tem-

perature, d is the distance between conducting layers (~18 Å in present case) and the $\xi_c(0)$ is coherence length along the c-axis. However, above T_0 the inequality, $W > d_0 \gg \xi_{ab}(T) > \xi_c(T)$, is still held. In HTS's this is a quasi-two dimensional 2D fluctuation region [1,4]. In this 2D region $\sigma'(T)$ is described by the MT term of the HL theory [6] in the case of well structured films [2] and by the LD model when structural defects are present in the sample [31].

We have followed the expression, $\sigma'(T) = \sigma_{RT}\varepsilon^{-\lambda D}$, for the fitting of resistivity versus temperature data for excess conductivity analyses in the neighborhood of transition regime and beyond. The dimensional exponent values λ_D and a cross over temperature from the log plot of the excess conductivity versus the reduced temperature are mentioned in Tables 1 and 2. The λ_{3D} refers to the exponent value below the T_0, the λ_{2D} to the value above T_0 and λ_{0D} correspond to exponent value of –2.0. The exponent λ_{0D} refers to the temperature point where Cooper pairs are born and broken down instantly and their formation is not supported in any preferred direction. The values of λ_{3D}, λ_{2D} and λ_{0D} for as-prepared samples are given in Table 1 whereas those for oxygen post-annealed samples are also given in Table 3. Due to predominant single phase nature of the samples we have assumed the small population of the defects in the CuO_2/ZnO_2 planes. From the cross-over temperature of λ_{2D} and λ_{0D} [from LD to Makki–Thompson (MT)] occurs at a temperature where, $\delta \cong \alpha$, which gives [7]:

$$\varepsilon_0 \cong (\pi\hbar)/[1.203(l/\xi_{ab})(8k_BT\tau_\varphi]. \quad (6)$$

When the sample is brought from lower to higher temperature, at a particular point the mean free path l of the Cooper's pair approaches ξ_{ab} and they are separated apart into Fermions. At this temperature (λ_{2D} and λ_{0D} cross-over temperature T) the phase relaxation time of the Cooper-pair is estimated as:

Table 1. The parameters extracted from the FIC analysis of as prepared $Cu_{0.5}Tl_{0.5}Ba_2Ca_3Cu_{4-y}Zn_yO_{12-\delta}$ (y = 0, 0.5, 1.5, 2.5) samples.

Sample	T_c, K	T_0, K	T_c^{mf}, K	$\alpha = \rho_n(0\text{ K})$, Ω·cm	λ_{3D} slope	λ_{2D} slope	λ_{0D} slope	$\xi_c(0)$, Å	$J = [2\zeta(0)]^2/d^2$
y = 0.0	99.3	108	102.1	0.02	–0.53	–1.2	–2.0	2.55	0.08
y = 0.5	103.4	116	109.4	0.30	–0.52	–1.3	–2.1	3.07	0.11
y = 1.5	110.4	115	111.3	0.02	–0.50	–1.4	–2.0	1.72	0.03
y = 2.5	106.6	117	112.3	0.09	–0.53	–1.3	–2.1	2.76	0.09

Table 2. The widths of 3D, 2D and 0D fluctuation regions observed from the fitting of the experimental data of as prepared $Cu_{0.5}Tl_{0.5}Ba_2Ca_3Cu_{4-y}Zn_yO_{12-\delta}$ (y = 0, 0.5, 1.5, 2.5) samples using AL model.

Sample	λ_{3D} Temperature	$\ln\varepsilon$ (Range in 3D)	λ_{2D} Temperature	$\ln\varepsilon$ (Range in 2D)	λ_{0D} Temperature	$\ln\varepsilon$ (Range in 0D)
y = 0.0	103–108	$-5.8 < \ln\varepsilon < -2.9$	108–142	$-2.9 < \ln\varepsilon < -0.9$	142–158	$-0.9 < \ln\varepsilon < -0.6$
y = 0.5	111–116	$-4.7 < \ln\varepsilon < -2.9$	116–139	$-2.9 < \ln\varepsilon < -1.3$	139–151	$-1.3 < \ln\varepsilon < -0.9$
y = 1.5	113–115	$-4.6 < \ln\varepsilon < -3.6$	115–136	$-3.6 < \ln\varepsilon < -1.5$	136–153	$-1.5 < \ln\varepsilon < -0.9$
y = 2.5	114–117	$-4.6 < \ln\varepsilon < -3.3$	117–146	$-3.3 < \ln\varepsilon < -1.2$	146–156	$-1.2 < \ln\varepsilon < -0.9$

Table 3. The parameters extracted from the FIC analysis of oxygen annealed $Cu_{0.5}Tl_{0.5}Ba_2Ca_3Cu_{4-y}Zn_yO_{12-\delta}$ (y = 0, 0.5, 1.5, 2.5) samples.

Sample	T_c, K	T_0, K	T_c^{mf}, K	$\alpha = \rho_n(0\text{ K})$, Ω·cm	λ_{3D} slope	λ_{2D} slope	λ_{0D} slope	$\xi_c(0)$, Å	$J = [2\zeta(0)]^2/d^2$
y = 0.0	111.4	117	114.2	0.050	–0.48	–1.3	–2.3	1.910	0.045
y = 0.5	109.4	122	116.0	0.056	–0.52	–1.3	–2.1	2.986	0.110
y = 1.5	112.3	116	113.2	0.010	–0.5	–1.0	–2.0	1.501	0.027
y = 2.5	112.3	120	114.2	0.025	–0.52	–1.2	–2.2	2.269	0.063

Table 4. The widths of 3D, 2D and 0D fluctuation regions observed from the fitting of the experimental data of oxygen annealed $Cu_{0.5}Tl_{0.5}Ba_2Ca_3Cu_{4-y}Zn_yO_{12-\delta}$ (y = 0, 0.5, 1.5, 2.5) samples using AL model.

Sample	λ_{3D} Temperature	$\ln\varepsilon$ (Range in 3D)	λ_{2D} Temperature	$\ln\varepsilon$ (Range in 2D)	λ_{0D} Temperature	$\ln\varepsilon$ (Range in 0D)
y = 0.0	115–117	$-6.2 < \ln\varepsilon < -3.9$	117–142	$-3.9 < \ln\varepsilon < -1.4$	142–153	$-1.4 < \ln\varepsilon < -1.0$
y = 0.5	117–122	$-5.8 < \ln\varepsilon < -3.1$	122–142	$-3.1 < \ln\varepsilon < -1.5$	142–147	$-1.5 < \ln\varepsilon < -1.3$
y = 1.5	114–116	$-6.5 < \ln\varepsilon < -3.9$	116–147	$-3.9 < \ln\varepsilon < -1.2$	147–157	$-1.2 < \ln\varepsilon < -0.9$
y = 2.5	115–120	$-6.2 < \ln\varepsilon < -3.1$	120–150	$-3.1 < \ln\varepsilon < -1.2$	150–155	$-1.2 < \ln\varepsilon < -1.0$

$$\tau_\varphi = \frac{\pi\hbar}{8k_B T\varepsilon_0} \quad (7)$$

The data of resistivity measurements for as-prepared $Cu_{0.5}Tl_{0.5}Ba_2Ca_3Cu_{4-y}Zn_yO_{12-\delta}$ (y = 0, 0.5, 1.5, 2.5) samples for each composition is also shown in the insets of Fig. 5 and for oxygen post-annealed samples in Fig. 6, respectively. In the inset of each figure, a derivative of the resistivity in the transition region is displayed showing a single peak reminiscence of single phase nature of material in each composition. The onset of excess conductivity starts at T^*, it is a temperature at which measured resistivity deviates from the extrapolated to zero Kelvin resistivity of defects; as-prepared $Cu_{0.5}Tl_{0.5}Ba_2Ca_3Cu_{4-y}Zn_yO_{12-\delta}$ samples have shown T^* values around 162.3, 166.3, 157.4, 159.3 K, respectively. At this temperature an onset of fluctuations in the order parameter of superconducting electrons sets in. All the as-prepared samples have shown a linear dependence of resistivity with temperature down to 166 K whereas this temperature is shrunk up to 187 K in the oxygen post-annealed samples. The T_0 is the temperature at which a cross over in the order parameter of the carriers from the 3D to 2D occurs. The as-prepared $Cu_{0.5}Tl_{0.5}Ba_2Ca_3Cu_{4-y}Zn_yO_{12-\delta}$ samples have shown T_0 around 108, 116, 115 and 117 K, respectively. The values of parameters such as T_c, T_c^{mf}, α and width of transition various transition regimes (3D, 2D etc) are listed in Tables 1 and 2 for as-prepared samples and Tables 3 and 4 for oxygen post-annealed samples. The parameter α determines intergrain connectivity and lower values are recommended for lower defects contribution to the residual resistivity of the sample. The α values determined for as-prepared $Cu_{0.5}Tl_{0.5}Ba_2Ca_3Cu_{4-y}Zn_yO_{12-\delta}$ samples are 0.02, 0.3, 0.02, and, 0.09 Ω·cm, respectively. However, these values determined for oxygen post-annealed samples are 0.05, 0,056, 0.01, 0.025 Ω·cm. A decrease in values of α may possibly be arising from the increased diffusion of oxygen both at the intra- and intergrain sites. The intragrain oxygen diffusion optimizes the carrier's concentration within the CuO_2/ZnO_2 planes whereas intergrain diffusion of oxygen promotes better interconnectivity and hence a decrease in the residual resistivity. The contribution of FIC to 3D and 2D excess conductivities have been

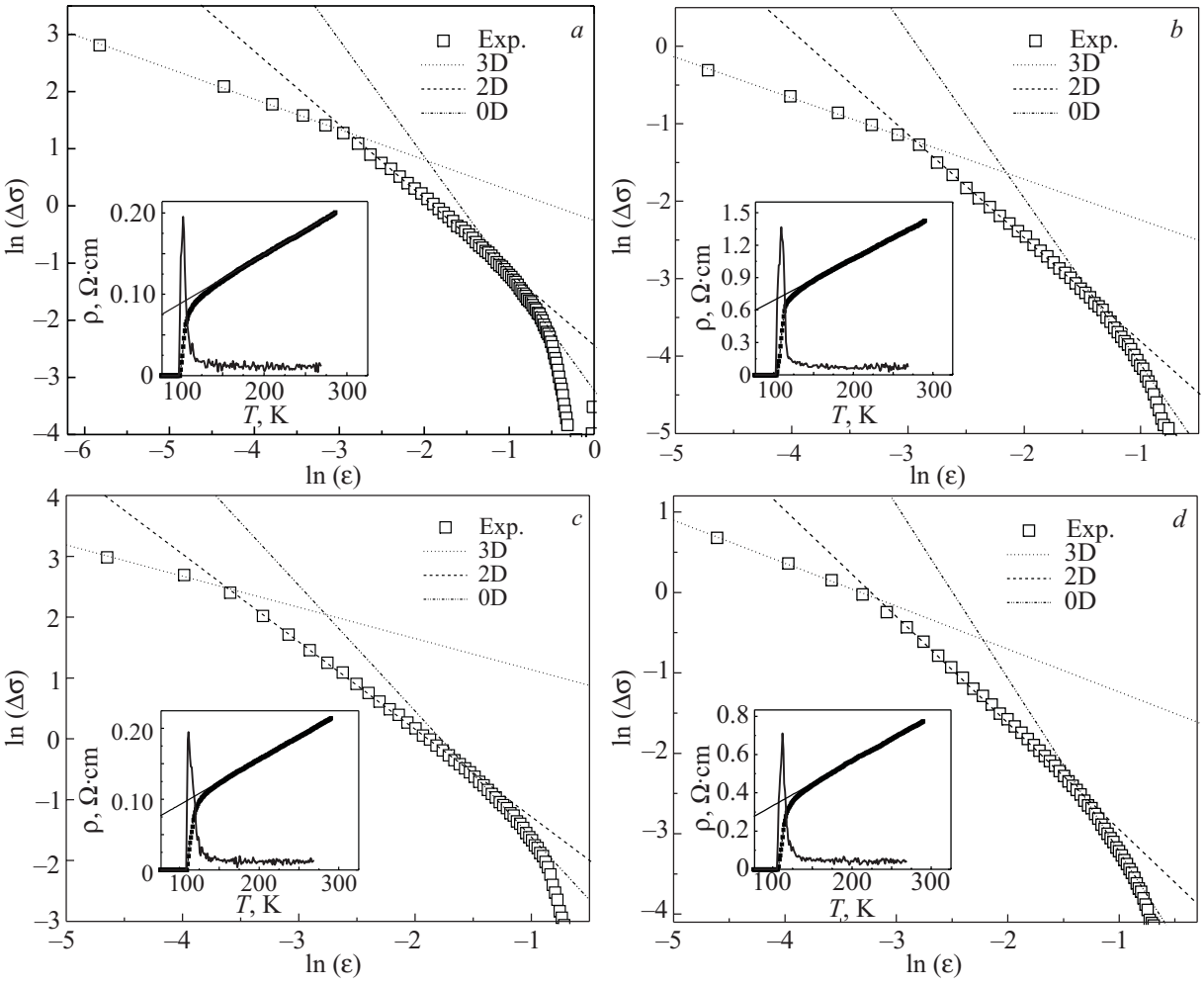

Fig. 5. ln (Δσ) versus ln (ε) plot of as prepared $Cu_{0.5}Tl_{0.5}Ba_2Ca_3Cu_{4-y}Zn_yO_{12-\delta}$ at different y: 0 (*a*); 0.5 (*b*); 1.5 (*c*); 2.5 (*d*).

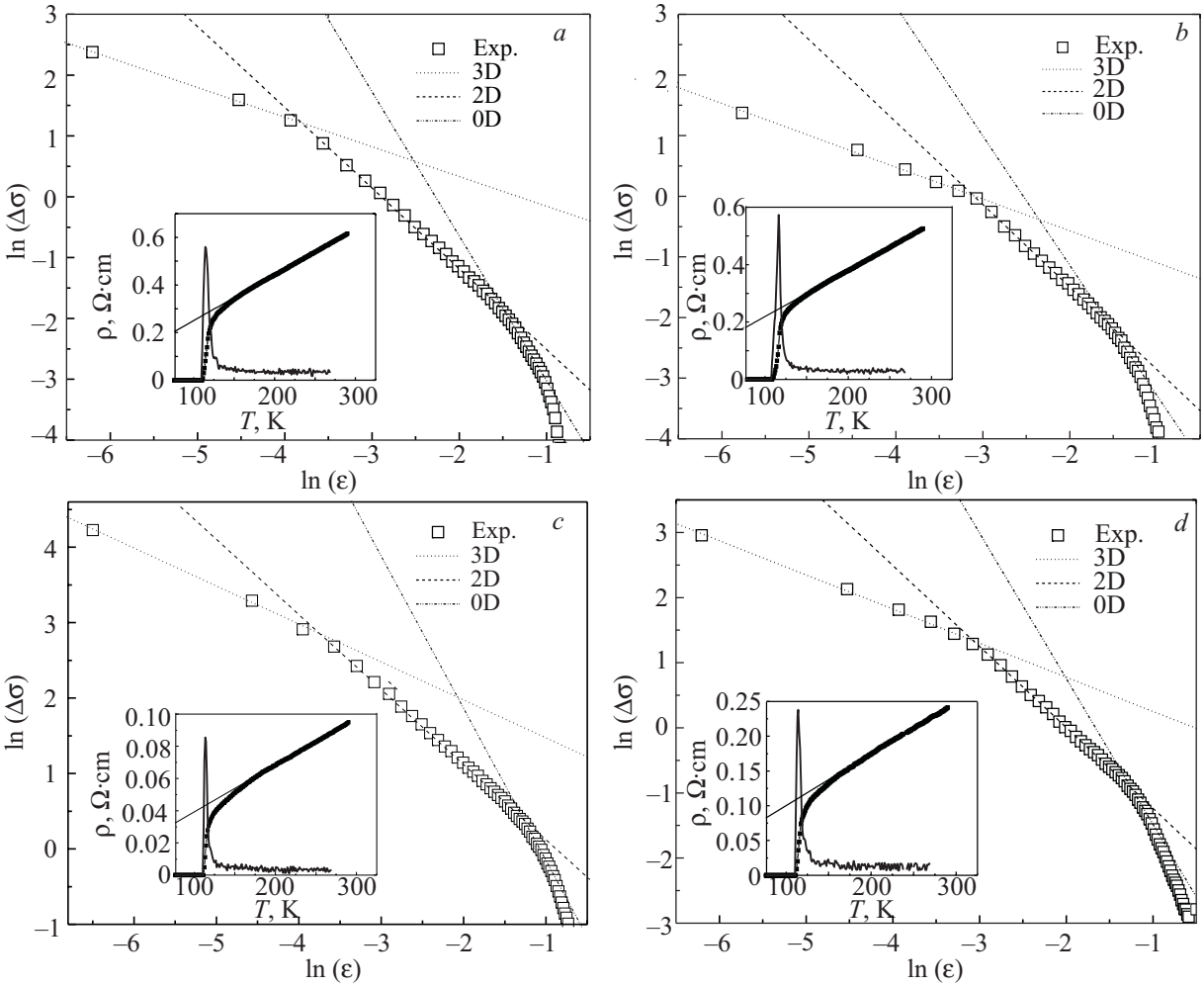

Fig. 6. ln (Δσ) versus ln (ε) plot of oxygen annealed $Cu_{0.5}Tl_{0.5}Ba_2Ca_3Cu_{4-y}Zn_yO_{12-\delta}$ sample at different y: 0 (*a*); 0.5 (*b*); 1.5 (*c*); 2.5 (*d*).

calculated by using the effective separation among the conducting CuO_2 planes "d = 18 Å" in this compound.

The λ_{3D} exponent values for as-prepared $Cu_{0.5}Tl_{0.5}Ba_2Ca_3Cu_{4-y}Zn_yO_{12-\delta}$ samples are found to be around –0.53, –0.52, –0.5, –0.53 in the temperature regimes 103–108, 111–116, 113–115 and 114–117 K, respectively (see Tables 1 and 2). This data showed 3D LD regime shifted to higher temperature values with the increased Zn-doping. It is most likely that increased population of doped spin-less Zn atoms in the CuO_2 planes suppress the scattering of the carriers which extend 3D LD region and shift it to higher temperatures, Fig. 5. The λ_{2D} exponent above the cross-over temperature T_0 for $Cu_{0.5}Tl_{0.5}Ba_2Ca_3Cu_{4-y}Zn_yO_{12-\delta}$ samples are –1.2, –1.3, –1.4, –1.3 in the temperature regimes 108–142, 116–139, 115–155 and 117–146 K, respectively. The λ_{0D} exponent beyond the termination of 2D regime for $Cu_{0.5}Tl_{0.5}Ba_2Ca_3Cu_{4-y}Zn_yO_{12-\delta}$ samples are –2.0, –2.1, –2.0, –2.1 extended in the temperature regime 142–158, 139–151, 136–153 and 146–156 K, respectively (see Tables 1 and 2).

The ln (σ′) versus ln (ε) plots of oxygen post-annealed $Cu_{0.5}Tl_{0.5}Ba_2Ca_3Cu_{4-y}Zn_yO_{12-\delta}$ (y = 0, 0.5, 1.5, 2.5) samples are shown in Fig. 6, respectively. The exponent values determined from these plots along with the width of 3D AL and 2D AL regimes are given in Table 1. The λ_{3D} exponent values for oxygen post-annealed $Cu_{0.5}Tl_{0.5}Ba_2Ca_3Cu_{4-y}Zn_yO_{12-\delta}$ (y = 0, 0.5, 1.5, 2.5) samples are –0.48, –0.52, –0.5, –0.52 in the temperature regimes 115–117, 117–122, 114–116 and 115–120 K, respectively. This data showed 3D AL regime shifted to higher temperature values with the increased Zn-doping. It is most likely that increased population of doped spin-less Zn atoms in the charge reservoir layer suppress the scattering of the carriers and 3D AL region is shifted to high temperatures, Fig. 6. The λ_{2D} exponent above the cross over temperature T_0 for $Cu_{0.5}Tl_{0.5}Ba_2Ca_3Cu_{4-y}Zn_yO_{12-\delta}$ samples are –1.3, –1.3, –1.0, –1.2 in the temperature regimes 117–142, 122–142, 116–147 and 120–150 K, respectively. The λ_{0D} exponent beyond the termination of 2D regime are –2.3, –2.1, –2.0, –2.2 and is extended in temperature regimes 142–153, 142–147, 147–157 and 150–155 K, respectively, see Tables 3, 4.

This is worth emphasizing that that the data of Fig. 5 and Fig. 6 becomes 3-dimensional [1,2]. This 3D temperature dependence of σ′ is described by the 3D AL equation

(3) as well. In $\ln \sigma'$ versus $\ln \varepsilon$ scale it is a straight line with the slope $\lambda \approx -0.5$. At T_0 there exists 3D–2D crossover as temperature increases. Simultaneously the fluctuating pairs scattering mechanism also changes [30,33]. As a result noticeably different $\sigma'(T)$ dependence is observed. Above the crossover temperature T_0 we can use both LD equation (1) and 2D AL equation (2) to fit the data. In our case, however, the much better LD fit is observed. The data of Fig. 5,*a* to a great extent gives a curved look whereas in Zn-doped samples in Figs. 5, 6 (*b*,*c*,*d*) look extremely linear in this temperature region. Such behavior is absent in high temperature superconductors and may possibly be arising due to the specific influence of Zn on the scattering mechanism which is realized in the compound under study.

By using the expressions of LD model for cross-over temperature $T_0 = T_c[1+(2\xi_c(0)/d)^2]$ and inter-layer coupling parameter $J = [2\xi_c(0)]^2/d^2$ are determined. The inter-layer distance d = 18 Å is between CuO_2/ZnO_2 planes is used for the calculations of these parameters of our $Cu_{0.5}Tl_{0.5}Ba_2Ca_3Cu_{4-y}Zn_yO_{12-\delta}$ samples [20]. The coherence length $\xi_c(0)$ along the *c*-axis for as-prepared and oxygen post-annealed samples are given in Tables 1 and 3. For $Cu_{0.5}Tl_{0.5}Ba_2Ca_3Cu_{4-y}Zn_yO_{12-\delta}$ as-prepared samples the $\xi_c(0)$ values are 2.664, 3.142, 1.837, 2.811 Å and J values are 0.088, 0.116, 0.042, 0.098, respectively (Table 1). Whereas, $\xi_c(0)$ = 2.018, 3.054, 1.698, 2.356 Å and J values 0.050, 0.115, 0.040 and 0.069 are observed for oxygen post-annealed $Cu_{0.5}Tl_{0.5}Ba_2Ca_3Cu_{4-y}Zn_yO_{12-\delta}$ (y = 0, 0.5, 1.5, 2.5) samples (Table 3). In comparison with undoped samples, the increase in the $\xi_c(0)$ values in the samples with Zn-doping of y = 0.5 is most likely associated with increased carrier's concentration in the CuO_2 planes which suppress antiferromagnetic order of Cu-spin [28] existing in the inner CuO_2 planes of $Cu_{0.5}Tl_{0.5}Ba_2Ca_3Cu_4O_{12-\delta}$ samples. A small suppression in the value of $\xi_c(0)$ in Zn-doped $Cu_{0.5}Tl_{0.5}Ba_2Ca_3Cu_{2.5}Zn_{1.5}O_{12-\delta}$ samples, may possibly be associated with the reordering of small spins of remaining Cu atoms in the CuO_2/ZnO_2 planes. It is most likely that when the number of doped Zn-atoms in the CuO_2 planes is less than 50%, the spins of Cu atoms in the CuO_2 planes stay anti-ferromagnetic aligned which suppress coherence length along the *c*-axis and inter-layer coupling J. The increase ratios of doped Zn-atoms in the CuO_2 planes beyond 50% significantly suppress the antiferromagnetic aligned spins of Cu-atoms and hence an increase in the values of $\xi_c(0)$ is observed. In oxygen post-annealed samples, a small decrease in the values of $\xi_c(0)$ and inter-layer coupling parameter J is reminiscence of decreased carrier concentration in the CuO_2/ZnO_2 planes promoted by intragrain diffusion of oxygen atoms in the unit cells. A decreased carrier density suppresses the Fermi-vector of the carrier and hence the coherence length along the *c*-axis.

A cross of LD-MT transition predicted in HL theory [6] is also witnessed in the log plot of the data of excess conductivity versus the reduced temperature. From the cross over of λ_{2D} and λ_{0D} (LD to MT transition) the phase relaxation time τ_φ of the Cooper pair is determined. By using this phase relaxation time the coupling constant $\lambda = \hbar\tau_\varphi^{-1}/(2\pi k_B T)$, the Fermi velocity of the carriers $v_F = 5\pi k_B T_c \xi_c(0)/(2K\hbar)$ ($K \cong 0.12$ is a coefficient of proportionality as used in reference [1]), and the energy required to break apart the Cooper pairs $E = h/\tau_\varphi(1.6\cdot10^{-19})$ are determined [8,29]. The values of τ_φ are in the range of 10^{-13} s which are comparable to the values found in other oxide superconductors. The coupling constant λ values are greater than 0.04 which manifested that priority mechanism of superconductivity in our samples is electron-phonon interaction and the electron-electron correlation effect is possibly minimal [29].

In the previous studies on Zn-doped samples it has been argued that there is localization of the carriers in at the Cu sites in the neighborhood of doped Zn atoms (at the planar sites). It was suggested in these studies that there is Anderson localization [19–24] of the carriers which suppresses the density of the mobile carriers essential for the superconductivity. A substantial increase in the normal state resistivity of $Cu_{0.5}Tl_{0.5}Ba_2Ca_3Cu_{4-y}Zn_yO_{12-\delta}$ (y = 0, 0.5, 1.5, 2.5) samples was expected, if such localization of the carriers would have occurred. None of such substantial changes are witnessed in the resistivity measurements. Originating from to the localization of the carriers, in the FIC analyses of our data, a substantial suppression of the coherence length along the *c*-axis due to possible suppression of density of the mobile carriers was expected. The value of $\xi_c(0)$ decreases in the samples with Zn-doping of y = 1.5, but the possible route causes of this suppression is most likely the competing ordering of small spins of the remaining Cu atoms in the CuO_2/ZnO_2 planes. Due to the doping of Zn, the suppression in the density of small spins of Cu atoms in the CuO_2/ZnO_2 planes is expected which in turn can suppresses the overall pseudo gap. This suppression would arise from the decreased contribution of the spin gap Δ_{sg}; since in the $\Delta_{pg} = \Delta_{cg}^2 + \Delta_{sg}^2 + \Delta_{NMR}^2 + \Delta_p^2$ [32]. The suppression in the pseudo-gap could be witnessed in the form of decrease in the energy E required to break apart the Cooper pairs, (see Table 5). However, the absolute value of this energy E is altered after post-annealing in oxygen. This change in the energy compliments our belief, since the concentration of the carriers in the conducting planes is optimized after post-annealing which suppress the spin's disorder in CuO_2/ZnO_2 planes. Since the Cooper-pairs are formed at the short length scale of the order of $\xi_c(0)$ and are separated form the normal electron by some energy gap. This gap is over all consequence of charge density gap Δ_{cg}, spin density gap Δ_{sg}, a gap having magnetic origin Δ_{NMR} and pairing gap Δ_p [32]. Sum of these four gap add up and form the pseudo

Table 5. The Fermi velocity v_F, phase-relaxation time for cooper pair t_φ, coupling constant λ, and energy require to break apart the Cooper pair of $Cu_{0.5}Tl_{0.5}Ba_2Ca_3Cu_{4-y}Zn_yO_{12-\delta}$ (y = 0, 0.5, 1.5, 2.5) as-prepared and oxygen post-annealed samples.

$Cu_{0.5}Tl_{0.5}Ba_2Ca_3Cu_{4-y}Zn_yO_{12-\delta}$	$v_F = \frac{5\pi k_B T_c \xi_c(0)}{2K\hbar}$, 10^7 cm/s	$\tau_\varphi = \frac{\pi\hbar}{8k_B T\varepsilon_0}$, 10^{-13} s	$\lambda = \frac{\hbar\tau_\varphi^{-1}}{2\pi k_B T}$	E, eV
y = 0.0 As-Prepared	2.26566	0.550244	0.15563	0.07526
y = 0.5 As-Prepared	2.78252	0.815708	0.10725	0.05077
y = 1.5 As-Prepared	1.73696	1.021960	0.08749	0.04052
y = 2.5 As-Prepared	2.56643	0.700255	0.11894	0.05914
y = 0.0 O_2-Annealed	1.92539	0.888679	0.09636	0.04660
y = 0.5 O_2-Annealed	2.86153	0.969837	0.08830	0.04270
y = 1.5 O_2-Annealed	1.63316	0.697857	0.11854	0.05934
y = 2.5 O_2-Annealed	2.26604	0.650701	0.12458	0.06364

gap, which determines the suppression of effective density of states above the critical temperature. The pseudo gap keep suppressing as a sample is brought from higher temperature towards T_c (onset). Around the transition temperature the regions of local pair formation, existing over the length scale of $\xi_c(0)$, coalesce resulting to a bulk superconductivity.

4. Conclusions

We have successfully synthesized superconductors $Cu_{0.5}Tl_{0.5}Ba_2Ca_3Cu_{4-y}Zn_yO_{12-\delta}$ (y = 0, 0.5, 1.5, 2.5) samples at 900 °C and studied their excess conductivity properties.

The incorporation of the Zn in the final compound is confirmed by the systematic softening of CuO_2 planar oxygen modes with increased concentration of doped atoms. These samples have shown tetragonal crystal structure and their c-axes length decreases with increased Zn concentration. The decreased c-axes length is also supported by the softening of apical oxygen phonon modes. The decreased c-axis length suppresses the volume of the unit cell which promotes an increase of the Fermi vector $k_F = (3\pi^2 N/V)^{1/3}$, the coherence length along c-axis $\xi_c = = (\hbar k_F/2m\Delta)$, and the Fermi velocity $v_F = (\pi\xi_c\Delta/\hbar)$ of the carriers [26]. The increase ξ_c and v_F most likely promotes enhancement in the $T_c(R = 0)$, magnitude of diamagnetism in Zn doped samples. The zero resistivity critical temperature is enhanced with the Zn-doping in the final compound which further increases with post-annealing in oxygen atmosphere. Since the density of the charged carriers supplied to the conducting CuO_2/ZnO_2 planes crucially depends on the ratios of Cu^{+2}/Tl^{+3} atoms in the $Cu_{0.5}Tl_{0.5}Ba_2O_{4-\delta}$ charge reservoir layers, therefore, their optimized density is achieved after post-annealing in the oxygen atmosphere. The presence of Cu^{+2} in the $Cu_{0.5}Tl_{0.5}Ba_2O_{4-\delta}$ charge reservoir layers of $Cu_{0.5}Tl_{0.5}Ba_2Ca_3Cu_{4-y}Zn_yO_{12-\delta}$ most efficiently dopes the CuO_2/ZnO_2 planes with carriers and we get enhanced superconductivity. Another most likely reason for the enhancement in the superconductivity parameters is decreased magnitude of Cu atoms with small spins consequently suppressing the spin scattering. Moreover, with the doping of Zn a decrease in the proportion of anti-ferromagnetic aligned spins of Cu atoms, existing in the inner CuO_2 planes, occurs which suppresses the spin density gap possibly existing in conducting CuO_2 planes, which most likely enhances the superconductivity in the final compound.

The FIC analysis is carried by employing LD model in the mean field region have shown that 3D LD regime along with the cross over temperature T_0 are shifted to higher temperatures with doping of Zn. The coherence length $\xi_c(0)$ and inter-layer coupling J in all Zn-doped samples, except the samples y = 1.5, are increased. It is most likely that in the samples with y = 1.5, number of Zn-atoms in the CuO_2 planes is less than 50%, the population of antiferromagnetic aligned Cu atoms stays dominant which suppress the carrier's concentration and hence coherence length along the c-axis. An increase ratios of doped Zn-atoms in the CuO_2 planes beyond 50% may suppress the antiferromagnetic aligned spins of Cu atoms in conducting CuO_2/ZnO_2 planes resulting into an enhancement in $\xi_c(0)$. A small decrease in the values of $\xi_c(0)$ and inter-layer coupling parameter J in oxygen post-annealed samples is most likely arising from the optimized carrier concentration CuO_2/ZnO_2 planes promoted by intragrain diffusion of oxygen in the unit cells.

It is unequivocally evidenced from these studies that the doped Zn $3d^{10}$ atoms at CuO_2 planar sites decrease the population of Cu $3d^9$ atoms with small spins which suppress the spin gap Δ_{sg} and hence the pseudo gap Δ_{pg} which is complemented by our FIC analysis of our data.

Acknowledgements

Higher Education Commission of Pakistan (HEC) through project No. 20–1482/R&D/09–1472 and Internal Center for Theoretical Physics (ICTP) through project

number PRJ–27 are acknowledged for their financial supports.

1. A.L. Solov'ev and V.M. Dmitriev, *Fiz. Nizk. Temp.* **35**, 227 (2009) [*Low Temp. Phys.* **35**, 169 (2009)].
2. A.L. Solovjov and V.M. Dmitriev, *Fiz. Nizk. Temp.* **32**, 139 (2006) [*Low Temp. Phys.* **32**, 99 (2006)].
3. L.G. Aslamazov and A.L. Larkin, *Phys. Lett*. **A26**, 238 (1968).
4. W.E. Lawrence and S. Doniach, *Proc. Twelfth Intern. Conf. Low Temp. Phys.*, Eizo Kanda (ed.), Keigaku, Tokyo (1971), p. 361.
5. K. Maki, *Prog. Theor. Phys.* **39**, 897 (1968); R.S. Thompson, *Phys. Rev.* **B1**, 327 (1970).
6. S. Hikami and A.I. Larkin, *Mod. Phys. Lett.* **B2**, 693 (1988); also in: B. Oh, K. Char, A.D. Kent, M. Naito, M.R. Beasley, T.H. Geballe, R.H. Hammond, A. Kapitulnik, and J.M. Grabeal, *Phys. Rev.* **B37**, 7861 (1988).
7. A.L. Solovjov, H.-U. Habermeier, and T. Haage, *Fiz. Nizk. Temp*. **28**, 24 (2002) [*Low Temp. Phys.* **28**, 17 (2002)].
8. A.L. Solovjov, H.-U. Habermeier, and T. Haage, *Fiz. Nizk. Temp*. **28**, 144 (2002) [*Low Temp. Phys.* **28**, 99 (2002)].
9. A.K. Ghosh, S.K. Bandyopadhyay, P. Barat, Pintu Sen, and A.N. Basu, *Physica* **C264**, 255 (1996).
10. T. Sato, H. Nakane, S. Yamazaki, N. Mori, S. Hirano, S. Yoshizawa, and T. Yamaguchi, *Physica* **C392–396**, 643 (2003).
11. Manmeet Kaur, R. Srinibasan, G.K. Mehta, D. Kanjilal, R. Pinto, S.B. Ogale, S. Mohan, and V. Ganesan, *Physica* **C443**, 61 (2006).
12. Mi-Ock Mun, Sung-Ik Lee, Sung-Ho Suck Salk, H.J. Shin, and M.K. Joo, *Phys. Rev.* **B48**, 6703 (1993).
13. Natsuki Mori John A.Wilson, and Hajimi Ozaki, *Phys. Rev.* **B45**, 10633 (1992).
14. S.H. Han and O. Rapp, *Solid State Commun.* **94**, 661 (1995).
15. Ajay Kumar Ghosh and A.N. Basu, *Phys. Rev.* **B59**, 11193 (1999).
16. P.P. Freitas, C.C. Tsuei, and T.S. Plaskett, *Phys. Rev.* **B36**, 833 (1987).
17. N. Goldenfeld, P.D. Olmsted, T.A. Friedmann, and D.M. Ginsberg, *Solid State Commun.* **65**, 465 (1988).
18. F. Vidal, J.A. Veira, J. Maza, and F. Miguelez, *Solid State Commun*. **66**, 421 (1988).
19. T.K.K. Radha, H.K.Barik, D. Bhattacharya, and K.L. Chopra, *Solid State Commun*. **74**, 1315 (1990).
20. J.L. Tallon, J.R. Cooper, P.S.I.P.N. de Silva, G.V.M. Willians, and J.W. Loram, *Phys. Rev. Lett.* **75**, 4114 (1995).
21. B. Nachumi, A. Keren, K. Kojima, M. Lakin, G.M. Luke, J. Merrin, O. Tchernyshov, Y.J. Uemura, N. Ichikawa, M. Goto, and S. Uchida, *Phys. Rev. Lett.* **77**, 5421 (1996).
22. D.N. Basov, B. Dabrowski, and T. Timusk, *Phys. Rev. Lett.* **81**, 2132 (1998).
23. N. Kakinuma, Y. Ono, and Y. Kokie, *Phys. Rev.* **B59**, 1491 (1999).
24. S.H. Pan, E.W. Hudson, K.M. Lang, H. Eisaki, S. Uchida, and J.C. Davis, *Nature (London)* **403**, 746 (2000).
25. Nawazish Ali Khan and Muhammad Mumtaz, *Phys. Rev.* **B77**, 054507 (2008).
26. M. Mumtaz and Nawazish A. Khan, *Supercond. Sci. Technol.* **21**, 65015 (2008).
27. Nawazish A. Khan, M. Zafar Iqbal, and N. Baber, *Solid State Commun*. **92**, 607 (1994).
28. M. Mumtaz and Nawazish A. Khan, *Physica* **B404**, 3973 (2009) and references therein.
29. A.L. Solovjov, V.M. Dmitriev, and H.-U. Habermeier, *Phys. Rev.* **B55**, 8551 (1997).
30. Andrei Mourachkine, in: *Room-Temperature Superconductivity*, published in arrangement with Cambridge International Science publishing UK (2008), p. 185.
31. Y.B. Xie, *Phys. Rev.* **B46**, 13997 (1992).